Recombination-Dominated Nonequilibrium Heat Transfer to Arbitrarily Catalytic Hypersonic Vehicles

G. R. Inger* and J. Elder†
Iowa State University, Ames, Iowa 50010

Application of an approximate theory of nonequilibrium stagnation-point boundary-layer flow on highly cooled blunt bodies, including a finite atom recombination rate on the surface, is presented. The analysis is based on the fact that recombination near the cold wall dominates the nonequilibrium behavior. Closed-form solutions for the atom concentration at the wall and heat transfer are obtained in terms of a composite Damköhler number representing the combined effects of homogeneous and heterogeneous reaction, in good agreement with the numerical results of Fay and Riddell. The use of this theory in parametric studies of nonequilibrium heating sensitivity to various design parameters is discussed in detail.

Nomenclature

C = Chapman-Rubesin constant, $\rho_w\mu_w/\rho_s\mu_s$
C_p = specific heat
H_D = $\alpha_s Leh_D/C_pTs$
h_D = specific dissociation energy of molecules
K_w = speed of catalytic atom recombination on body surface
k_r' = recombination rate constant
Le = Lewis number, Pr/Sc
Pr = Prandtl number
P = static pressure
Q_w = nondimensional heat transfer rate, Eq. (10)
$\dot{q}_w$ = surface heat transfer rate per unit area
R_b = nose radius of curvature, Fig. 1
R_m = molecular gas constant
R_u = universal gas constant
$\mathcal{R}$ = net reaction rate distribution function, $\theta^{\omega-2}G$
r_o = local body radius, Fig. 1
Sc = Schmidt number
T = absolute temperature
z = α/α_s
α = atom mass fraction
β_s = inviscid flow stagnation-point velocity gradient, $(du/dx)_s$
Γ_c = composite Damköhler number for combined gas phase surface reaction, Eq. (9)
Γ_G = Damköhler number for gas-phase recombination, Eq. (4)
ϵ = shape parameter ($\epsilon = 0$, two-dimensional; $\epsilon = 1$, axisymmetric)
η = boundary-layer similarity coordinate
θ = T/T_s
θ_D = $h_D/(R_mT_s)$, characteristic dissociation temperature
μ = coefficient of viscosity
ρ = mixture density
ω = recombination rate temperature-dependence exponent, $k_r = k_r'T^\omega$

Subscripts

A = atom
EQ = equilibrium boundary-layer flow
F = frozen boundary-layer flow
M = molecule
s = inviscid flow conditions at stagnation point
w = condition on body surface

Presented as Paper 89-1859 at the AIAA 20th Fluid Dynamics, Plasma Dynamics, and Lasers Conference, Buffalo, NY, June 12-14, 1989; received June 28, 1989; revision received June 15, 1990; accepted for publication June 15, 1990.

*Professor, Department of Aerospace Engineering.
†Graduate Student, Department of Aerospace Engineering.

Introduction

THE combined effects of finite surface atom catalysis and nonequilibrium gas-phase dissociation-recombination on heat transfer are of major importance in the aerothermodynamics design of a variety of hypervelocity flight vehicles operating at high altitudes above 100,000 ft. Their study is of particular interest within the highly cooled recombination-dominated laminar boundary-layer flow around wing leading edge and nose regions of the proposed National Aerospace Plane configuration. In this connection, there is a need for a computationally efficient approximate method of determining the nonequilibrium heat transfer to conduct design-tradeoff studies.

Accordingly, this paper describes the application of a basic analysis of the nonequilibrium dissociated boundary layer on the arbitrarily catalytic nose-region surface which yields an analytic yet accurate preliminary design tool for determining the relative nonequilibrium heat transfer and wall atom concentration over a wide range of aerothermodynamic flight conditions. The resulting prediction method interpolates between the extremes of chemically frozen and dissociative equilibrium gas-phase behavior based on two nondimensional reaction-rate parameters (Damköhler numbers) that indicate the degree of relative nonequilibrium gas-phase reaction and finite surface catalysis, respectively. The use of this analysis is illustrated by an extensive parametric study showing how the combined gas-phase/surface-reaction effects on the nondimensional heat transfer depend on various design parameters such as body size and wall temperature, flight altitude and speed, and the chemical rate data.

Theoretical Analysis

Assumptions and Formulation

We consider nonequilibrium-dissociated airflow in the shock layer behind the bow shock around a highly cooled wing leading edge or body nose region (Fig. 1) under such hypervelocity flight conditions that the postshock dissociative and vibrational chemistry is fully equilibrated upon reaching the boundary-layer edge (i.e., we consider that wide range of altitude/speed flight conditions in which the dissociative relaxation time across the shock layer is very short compared to the atom recombination time within either the boundary layer or upon the body surface). The analysis of this problem may then be considerably simplified without loss of the essential

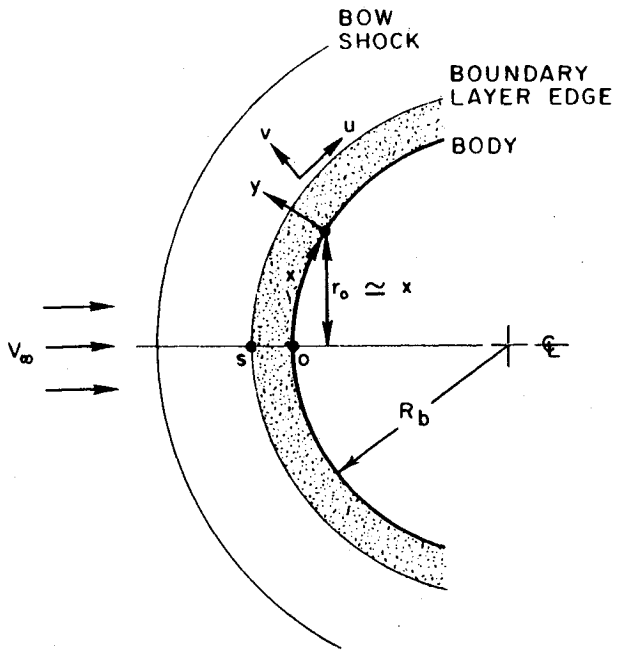

Fig. 1 Stagnation region flow configuration.

nonequilibrium flow thermophysics by introducing the following assumptions:

1) As far as heat transfer is concerned, the gas mixture is adequately approximated by a binary mixture of atoms and molecules with equal specific heats and negligible thermal diffusion between them.

2) Prandtl number, Schmidt number, and viscosity density product are all constant across the boundary layer.

3) Chemical reaction effects on the nondimensional self-similar velocity profile (via the density coefficient of the pressure gradient term in the momentum equation) are negligible enough to permit taking this profile as a known distribution in the leading approximation.

4) Finite catalytic atom recombination at the cold body surface is governed by a first-order rate law with negligible heterogeneous back dissociation.

The nonequilibrium boundary-layer problem in the stagnation region of a symmetric nose shape can then be formulated in terms of the similarity coordinate

$$\eta \equiv \sqrt{\frac{\rho_s(1+\epsilon)\beta_s}{C\mu_s}} \int_0^y \frac{\rho}{\rho_s}\,dy \tag{1}$$

so as to obtain the following atom mass and thermal energy conservation equations, respectively:

$$Scfz' + z'' = \frac{a_s}{1+a_s}\,\Gamma_G \mathcal{R}(z,\theta) \tag{2}$$

$$Prf\theta' + \theta'' = -\frac{a_s}{1+a_s}\,\Gamma H_D \mathcal{R}(z,\theta) \tag{3}$$

where a prime denotes differentiation with respect to η, $f(\eta)$ is the similarity stream function such that $U/U_e = f'(\eta)$, $\mathcal{R}(z,\theta)$ is a nondimensional net reaction rate defined below, and

$$\Gamma_G \equiv \frac{4k_r' T_s^{\omega-2} Sc}{(1+\epsilon)\beta_s}\left(\frac{p_s}{R_u}\right)^2 \tag{4}$$

is the characteristic (flow time/recombination time) ratio or gas-phase Damköhler number for the boundary layer. For a mixture of atoms and molecules undergoing the dissociation-recombination reaction,

$$A_2 + X \underset{K_r}{\overset{K_d}{\rightleftharpoons}} 2A + X \tag{5}$$

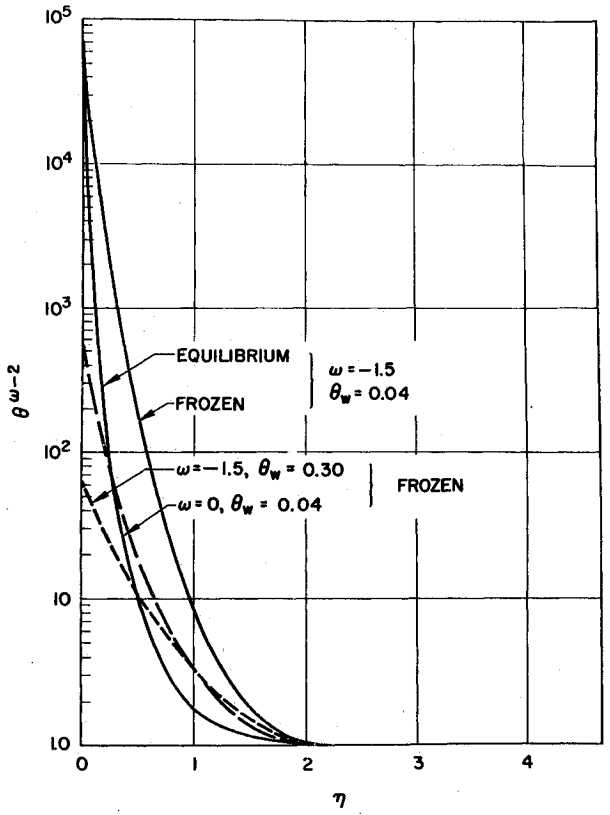

Fig. 2 Typical boundary-layer profile of the recombination-rate temperature dependence.

where A_2, A, and X denote a molecule, atom, and any third body, respectively, and $K_r = k_r' T^\omega$ is the recombination rate. $\mathcal{R}(z,\theta)$ can be written as

$$\mathcal{R}(z,\theta) \equiv \theta^{\omega-2} G(z,\theta) \cong \theta^{\omega-2}\left(\frac{1+a_s}{1+a_s z}\right) \times \left\{\underbrace{z^2}_{\text{recombination}} - \underbrace{\left(\frac{1-a_s^2 z^2}{1-a_s^2}\right)\exp\left[\frac{-\theta_d}{\theta}(1-\theta)\right]}_{\text{dissociation}}\right\} \tag{6}$$

where the function $\theta^{\omega-2}$ represents the effect of the varying temperature on the recombination rate (and pre-exponential portion of the dissociation rate). In view of the current evidence that $\omega \cong -1.5$ for air and most diatomics,[1] this effect dominates the nonequilibrium behavior across a highly cooled boundary layer (Fig. 2). The remaining function $G(z,\theta)$ indicated in Eq. (6) is of order unity or less and represents the composition-dependent part of the net atom reaction rate across the layer involving a contribution from both the local recombination and dissociation rates; it vanishes identically when the boundary layer is in complete equilibrium ($\Gamma_G \to \infty$) but does not in the opposite extreme of chemically frozen flow ($\Gamma_G \to 0$).

The boundary conditions on the solution to Eqs. (2) and (1) are as follows:

$$z(\infty) = \theta(\infty) = 1 \tag{7}$$

$$\theta(0) = \theta_w \qquad \text{(given)} \tag{8}$$

while on the arbitrarily catalytic surface

$$z'(0) = \underbrace{\frac{ScK_w}{\mu_w}\sqrt{\frac{C\rho_s\mu_s}{(1+\epsilon)\beta_s}}}_{\Gamma_c} z(0) \tag{9}$$

where Γ_c is the characteristic diffusion to recombination time ratio (heterogeneous Damköhler number) appropriate to stagnation flow, in terms of the atom recombination velocity K_w on the surface (a known function of the wall temperature and material[2]) which is in turn related to the catalytic efficiency γ_w by $\gamma_w = (K_w/R_m T_w)^{1/2}$. Condition (9) expresses the fact that the rate of atom diffusion from the gas to the wall is balanced by the rate of catalytic recombination on the surface. When $\Gamma_c \to \infty$, the surface is completely catalytic [$z(0) = 0$], whereas in the other extreme $\Gamma_c \to 0$, the surface is noncatalytic and atom diffusion into the wall vanishes [$z'(0) = 0$]. In what follows, arbitrary values of Γ_c are considered.

Once Eqs. (2–9) are solved for the atom concentration and temperature distributions, the surface heat transfer rate may be computed from

$$\frac{\left(-\frac{Pr\dot{q}_w}{C_{p,M}T_s}\right)}{\sqrt{\left(\frac{1+\epsilon}{2}\right)C\rho_s\mu_s\beta_s}} \equiv Q_w = \underbrace{\theta'(0)}_{\text{conduction}} + \underbrace{H_D z'(0)}_{\text{diffusion}} \tag{10}$$

Clearly, only heat conduction contributes to the heat transfer when the wall is completely noncatalytic or when the energy in dissociation is negligible.

Approximate Analytical Solution

An approximate yet accurate solution for the surface properties under arbitrary nonequilibrium conditions can be obtained as follows. First we perform a purely formal double integration of Eqs. (2) and (3) with respect to η to obtain, after applying the boundary conditions and carrying out some algeba, the relations

$$\frac{z(0)}{z_F(0)} = \frac{z'(0)}{z'_F(0)} = 1 - \frac{a_s\Gamma}{1+a_s}\,\mathcal{I}_z(\infty) \tag{11}$$

$$\theta'(0) = \frac{1-\theta_w + [a_s\Gamma H_D/(1+a_s)]\mathcal{I}_\theta(\infty)}{I_\theta(\infty)} = \frac{1-\theta_w}{I_\theta(\infty)} + \frac{H_D\mathcal{I}_\theta(\infty)}{I_\theta(\infty)I_z(\infty)}\left[1 - \frac{z(0)}{z_F(0)}\right] \tag{12}$$

$$z_F(0) = \frac{z'_F(0)}{\Gamma_c} = [1 + \Gamma_c I_z(\infty)]^{-1} \tag{13}$$

$$I_z(\eta) \equiv \int_0^\eta \exp\left(-Sc\int_0^\eta f\,d\eta\right) d\eta, \qquad I_z(\infty) \cong (0.47Sc^{1/3})^{-1} \tag{14}$$

$$\mathcal{I}_z(\eta) \equiv \int_0^\eta \exp\left(-Sc\int_0^\eta f\,d\eta\right)\left[\int_0^\eta \exp\left(Sc\int_0^\eta f\,d\eta\right)\mathcal{R}\,d\eta\right] d\eta \tag{15}$$

where z_F is the frozen flow solution for arbitrary surface catalycity while I_θ and $\mathcal{I}_\theta$ are obtained from Eqs. (14) and (15), respectively, by replacing Sc by Pr in the exponentials. Second, for highly cooled walls we apply the fact that the ratio $\mathcal{I}_\theta/\mathcal{I}_z$ is a weak function of Le only and further use the knowledge that the first two terms on the right side of Eq. (12) are equal to the equilibrium wall temperature gradient; Eqs. (11) and (12) consequently yield the following simple nondimensional ratio relationships:

$$1 - \frac{z(0)}{z_F(0)} = 1 - \frac{z'(0)}{z'_F(0)} = \frac{\theta'(0) - \theta'_F(0)}{\theta'_{EQ}(0) - \theta'_F(0)} = \frac{Q_w - Q_{w,F}}{Q_{w,EQ} - Q_{w,F}} \tag{16}$$

regardless of the values of Sc, Pr, Γ_G, or Γ_c. Equation (16) indicates that the solution to the species conservation equation is sufficient to determine all of the nonequilibrium conditions at the surface once the frozen and equilibrium values are known. Third, we take advantage of a very detailed study[3] of the net reaction-rate function for highly cooled walls with either catalytic or noncatalytic surfaces which showed that the recombination-dominated nature of the chemistry leads to the following convenient yet accurate approximation over the entire range of nonequilibrium behavior:

$$\mathcal{R} \simeq \left[\frac{1+\alpha_s}{1+\alpha_s z(0)}\right]\theta_F^{\omega-2}\left\{z^2(0) + \frac{2z(0)z'(0)}{0.47Sc^{1/3}}g_z + \left[\frac{z'(0)g_z}{0.47Sc^{1/3}}\right]^2\right\}\left\{1 - \exp\left[-\frac{\theta_D}{\theta_F}(1-\theta_F)\right]\right\} \tag{17a}$$

$$g_z(\eta) \equiv \left[\frac{I_z(\eta)}{I_z(\infty)}\right] \tag{17b}$$

which in turn gives from Eq. (15) the value

$$\mathcal{I}_z(\infty) \simeq \left[\frac{1+\alpha_s}{1+\alpha_s z(0)}\right]\left\{z^2(0)\mathcal{I}_{z,F_1} + \frac{2z(0)z'(0)}{0.47Sc^{1/3}}\mathcal{I}_{z,F_2} + \left[\frac{z'(0)}{0.47Sc^{1/3}}\right]^2\mathcal{I}_{z,F_3}\right\} \tag{18}$$

where

$$\mathcal{I}_{z,F_1} \equiv \int_0^\infty \exp\left(-Sc\int_0^\eta f\,d\eta\right)\left\{\int_0^\eta \exp\left(Sc\int_0^\eta f\,d\eta\right)\theta_F^{\omega-2} \times \left[1 - \exp\left(-\frac{\theta_D}{\theta_F}(1-\theta_F)\right)\right]d\eta\right\} d\eta \tag{19a}$$

$$\mathcal{I}_{z,F_2} \equiv \int_0^\infty \exp\left(-Sc\int_0^\eta f\,d\eta\right)\left\{\int_0^\eta \exp\left(Sc\int_0^\eta f\,d\eta\right)\theta_F^{\omega-2} \times \left[g_z(\eta) - \exp\left(-\frac{\theta_D}{\theta_F}(1-\theta_F)\right)\right]d\eta\right\} d\eta \tag{19b}$$

$$\mathcal{I}_{z,F_3} \equiv \int_0^\infty \exp\left(-Sc\int_0^\eta f\,d\eta\right)\left\{\int_0^\eta \exp\left(Sc\int_0^\eta f\,d\eta\right)\theta_F^{\omega-2} \times \left[g_z^2 - \exp\left(-\frac{\theta_D}{\theta_F}(1-\theta_F)\right)\right]d\eta\right\} d\eta \tag{19c}$$

are known reaction-rate integrals based solely on frozen-flow solutions that have been extensively evaluated and tabulated by the author: typical values, which are insensitive to small variations in Sc and Pr, are presented in Figs. 3a–3c. Substitution of Eq. (18) into Eq. (11) then yields a simple quadratic equation for the surface nonequilibrium atom concentration (hence the diffusion and heat flux) with arbitrary Γ_c whose solution is

$$Z \equiv \frac{z(0)}{z_F(0)} = \frac{z'(0)}{z'_F(0)} = \frac{\sqrt{[1 + a_s z_F(0)]^2 + 4\Gamma^*} - [1 - a_s z_F(0)]}{2[a_s z_F(0) + \Gamma^*]} \tag{20a}$$

where

$$\Gamma^* = a_s\left[\frac{\mathcal{I}_{z,F_1} + \frac{2\Gamma_c\mathcal{I}_{z,F_2}}{0.47Sc^{1/3}} + \frac{\Gamma_c^2\mathcal{I}_{z,F_3}}{(0.47Sc^{1/3})^2}}{\left(1 + \frac{\Gamma_c}{0.47\,Sc^{1/3}}\right)^2}\right]\Gamma_G \tag{20b}$$

is a composite Damköhler number representing the simultaneous effects of the finite gas-phase and surface reaction rates, as well as the influence of wall temperature and all of the thermochemical properties of the gas. The corresponding wall heat transfer is then obtained from Eq. (16).

Some Important Properties of the Solution

The solution (20) is plotted vs Γ^* in Fig. 4, from which it is seen that it is very insensitive to the parameter $\alpha_s z_F(0)$ and,

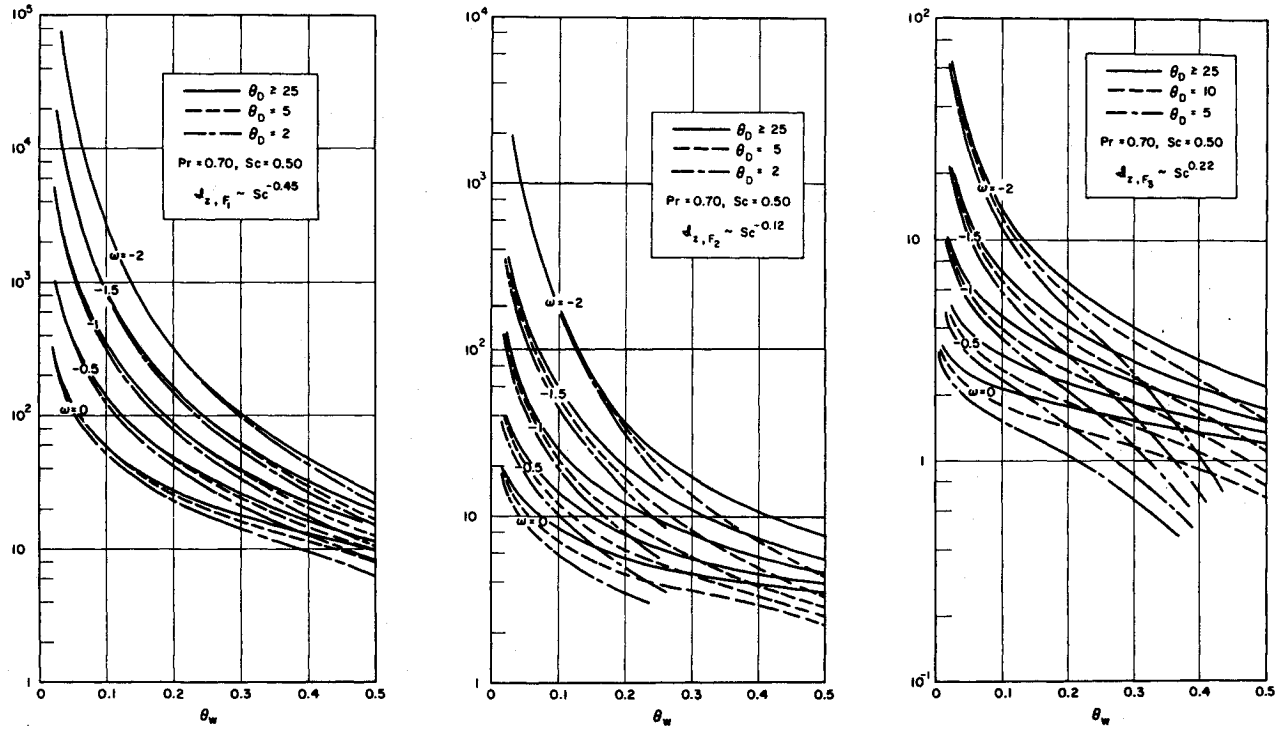

a) $\mathcal{I}_{z,F_1}$ b) $\mathcal{I}_{z,F_2}$ c) $\mathcal{I}_{z,F_3}$

Fig. 3 Reaction-rate integrals for stagnation-point flow.

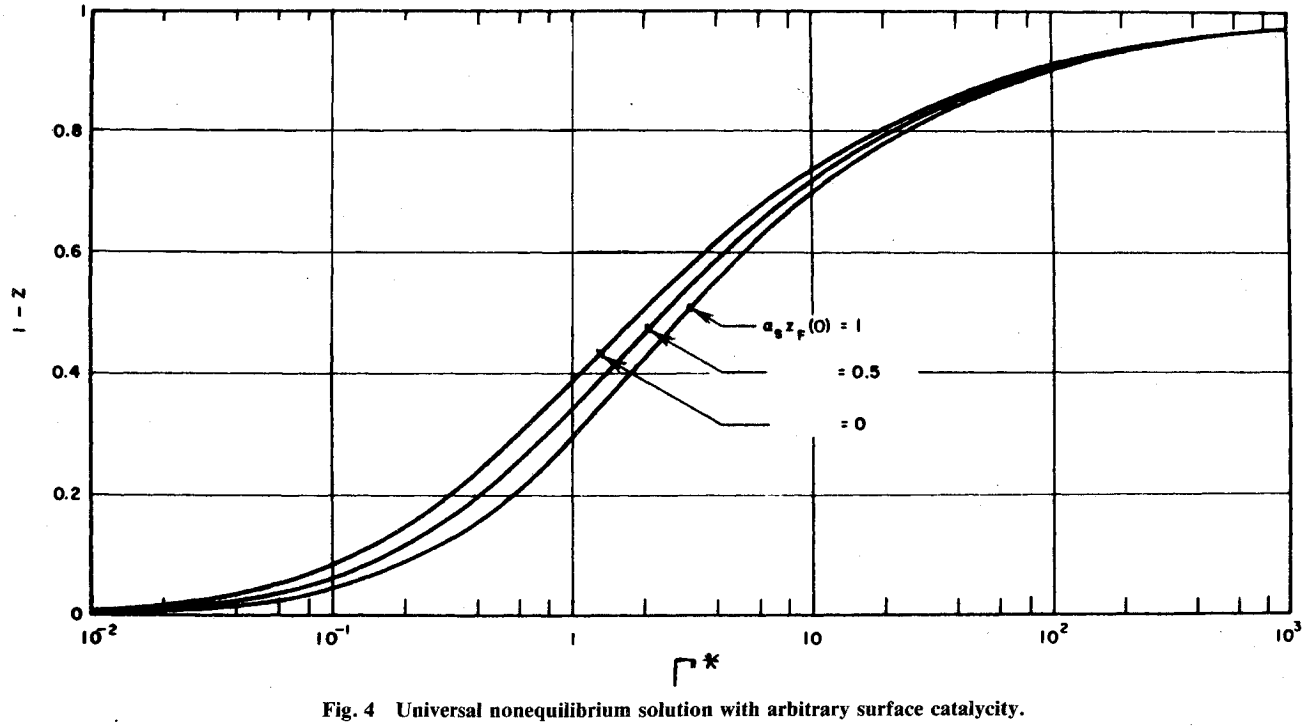

Fig. 4 Universal nonequilibrium solution with arbitrary surface catalycity.

hence, essentially a universal function of Γ^* alone. Thus, the relationships from Eqs. (16) and (20) that

$$\frac{Q_w - Q_{w,F}}{Q_{w,EQ} - Q_{w,F}} \simeq 1 - Z(\Gamma^*) \tag{21a}$$

$$\frac{z(0)}{z_F(0)} \simeq Z(\Gamma^*) \tag{21b}$$

in fact constitute a nonequilibrium similitude law for combined gas-phase/catalytic surface reaction effects in the recombination-dominated case.

Another noteworthy property is that Eq. (20) compares well with Fay and Riddell's exact numerical results[1] for arbitrary Γ_G: Fig. 5 illustrates the present prediction of nonequilibrium heat transfer vs both Γ_G and Γ_c for a typical case, where it can be seen to lie close to their results over the entire range of nonequilibrium effect in both the fully catalytic and com-

pletely noncatalytic wall extremes. Detailed discussion of further aspects of these comparisons can be found in Ref. 3.

Application to Parametric Studies of Nonequilibrium Stagnation Heating

The closed form of the foregoing analysis not only provides valuable physical insight but also a very efficient computational model of design parameters that influence the relative nonequilibrium effect on heat transfer. In particular, it can be used as an interpolative relationship between any frozen and equilibrium heat transfer solution routines the user wishes to supply. In the present work, we have used

$$Q_{w,EQ} \simeq 0.47 Pr^{1/3}[1 - \theta_w + Le^{-0.48} \times H_D] \tag{22}$$

$$Q_{w,F} \simeq 0.47 Pr^{1/3}\left[1 - \theta_w + Le^{-0.33} \times H_D\left(\frac{\Gamma_c}{0.47 Sc^{1/3} + \Gamma_c}\right)\right] \tag{23}$$

but it is emphasized that purely numerical values from any appropriate aerodynamic heating code would serve equally well in the application of Eqs. (16) and (20). With the preceding as a basis, we have performed an extensive parametric study of nonequilibrium heat transfer (and surface atom concentration) to illustrate its sensitivity to various important physical properties related to the vehicle size, the flight corridor conditions, and the chemical rate data. In carrying this out, the stagnation-point velocity gradient β_s was evaluated from the relationship

$$\beta_s \simeq R_b^{-1}\sqrt{\frac{2(p_s - p_\infty)}{\rho_\infty}} \tag{24}$$

whereas the equilibrium dissociated-air properties behind the (normal) bow shock and the attendant coefficient of viscosity values were determined from Refs. 4–7 in conjunction with the atmospheric data cited in Ref. 5. The assumed gas-phase and catalytic surface-rate values will be indicated in the figures cited presently.

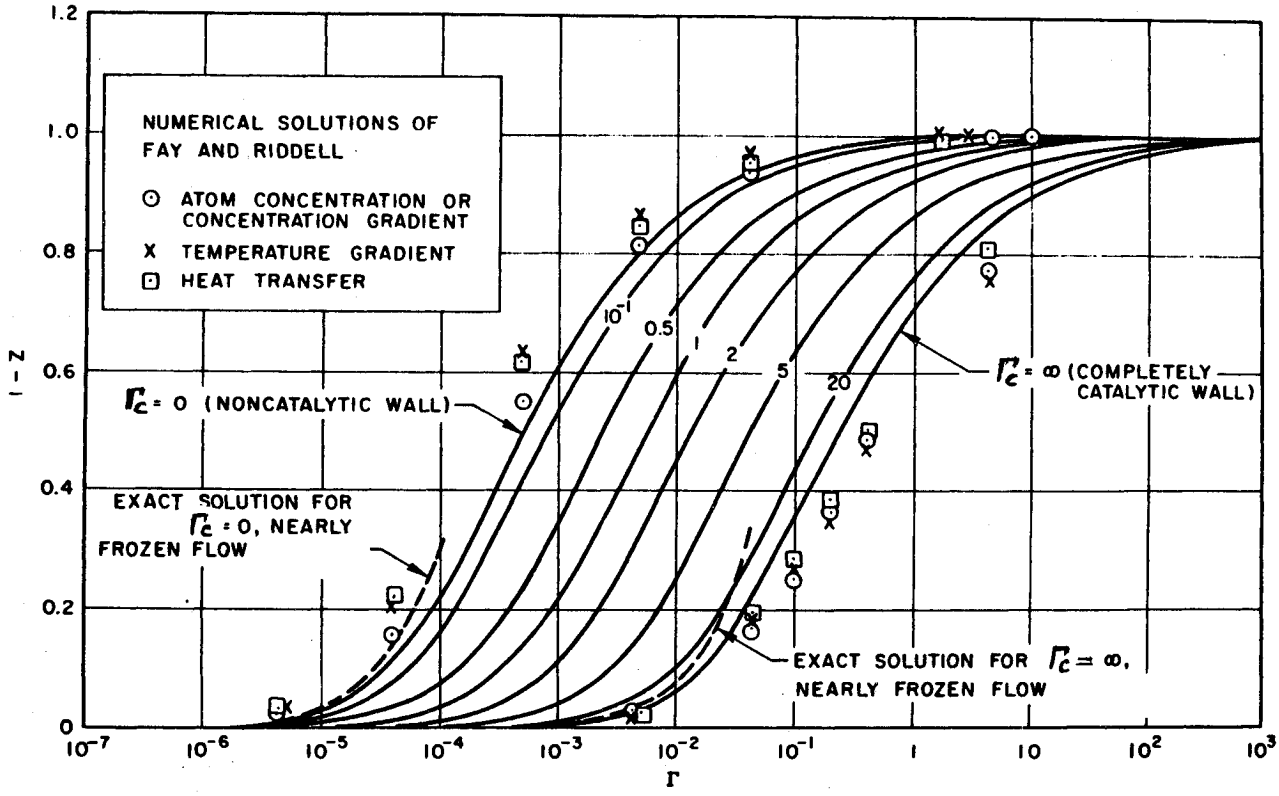

Fig. 5 Comparison of approximate analytical solution with exact numerical results.

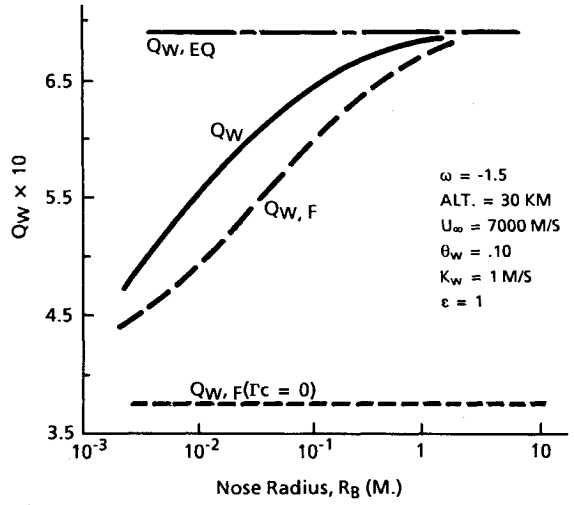

Fig. 6 Influence of nose radius on relative nonequilibrium heating.

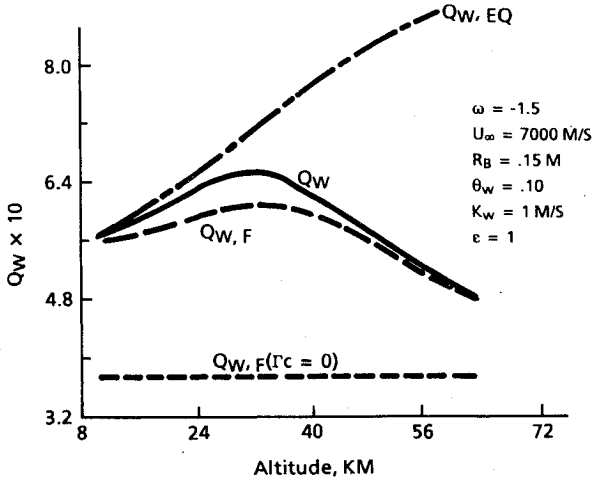

Fig. 7 Flight-altitude effect on the nonequilibrium heating.

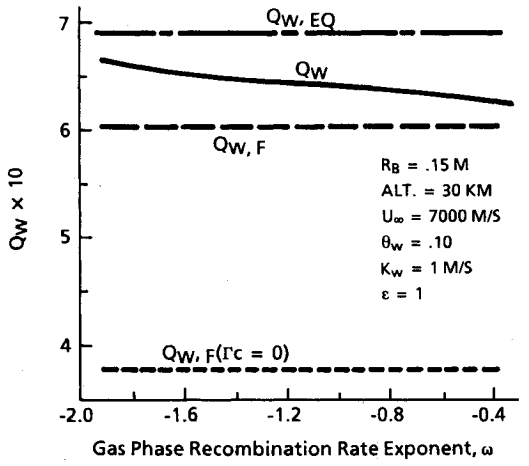

Fig. 8 Sensitivity of nonequilibrium heat transfer to the gas-phase recombination rate exponent.

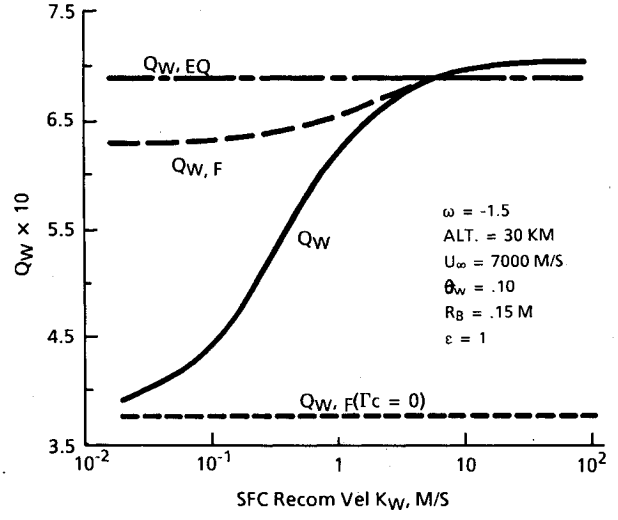

Fig. 9 Sensitivity of nonequilibrium heat transfer to the surface recombination rate parameter K_w.

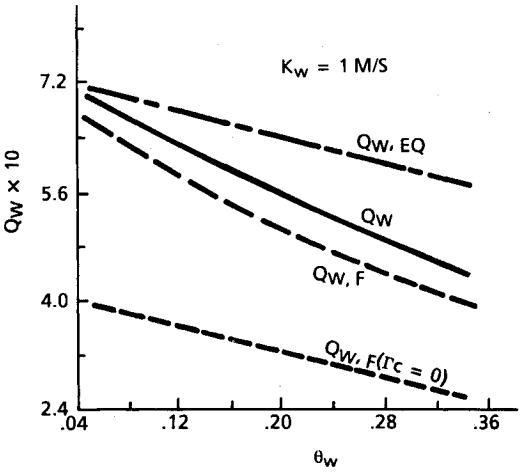

Fig. 10 Wall-temperature effect on nonequilibrium heating.

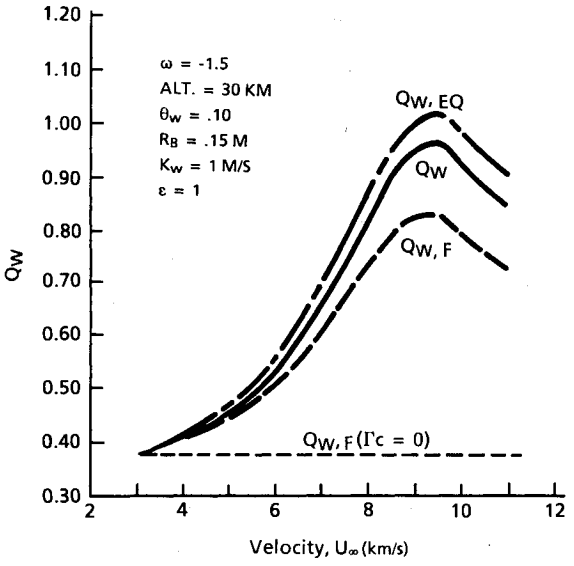

Fig. 11 Flight-velocity effect on nonequilibrium heating.

As a first example of results, Fig. 6 illustrates the predicted influence of increasing the nose radius R_b on the nonequilibrium heat transfer compared to the corresponding values based on the assumption of either full dissociative equilibrium or chemically frozen behavior (both arbitrarily catalytic and noncatalytic), all at the same nominal flight condition of $U_\infty = 7000$ m/s at 30-km altitude. It is seen that increasing R_b drives the heat transfer toward a more fully catalytic, equilibrium gas-phase behavior; physically, this is explained by the fact that both the surface area available for recombinative catalysis and the gas-phase recombination residence time increase with R_b.

A second example, illustrated in Fig. 7, shows the influence of flight altitude for a fixed velocity and body size: it is seen that as a result of the reduced density, increasing altitude results in a relative "freezing-out" of both the gas-phase and surface catalysis effects [in spite of the rise in $Q_{w,EQ}$ caused by the increase of H_D with altitude; see Eq. (22)].

Third, Fig. 8 shows the sensitivity of the gas-phase recombination rate temperature-dependence exponent ω. Noting from Eq. (6) and Fig. 2 that the relative net reaction rate per unit density in the highly cooled boundary-layer region near the wall is proportional to θ_w^ω with $\omega \approx -1.5$, we see for $\theta_w \ll 1$ that increasing ω toward positive values reduces gas-phase atom recombination in this region and so drives the heat transfer toward the frozen value pertaining to the prevailing level of surface catalysis. Such results bring out the value of the present theory in assessing acceptable rate-data accuracy for any desired engineering accuracy of nonequilibrium heat transfer prediction. This is further emphasized in Fig. 9, where results are shown for the sensitivity to the catalytic rate constant K_w. Here it can be seen as expected that the frozen flow heat transfer value rises rapidly with increased K_w (due, for example, to a change in surface material from a glassy type toward an oxide or pure metal) because of the enhanced atom diffusion rate of heat into the wall. Since the resulting increase in Γ_c also enhances the net effective Damköhler number Γ^* governing the gas-phase recombination rate effect, a corresponding rise toward equilibrium of the nonequilibrium heat transfer also occurs.

A fourth parametric study, regarding the important influence of the wall temperature ratio $\theta_w \cong T_w/T_s$, is summarized in Fig. 10. In addition to the obvious linear θ_w dependence of both $Q_{w,EQ}$ and $Q_{w,F}$ contained in Eqs. (22) and (23), wall temperature also influences both Γ_G and Γ_c and hence the combined gas-phase/surface catalysis nonequilibrium situation. Because of the viscosity-temperature dependence, $\Gamma_c \sim \theta_w^{1.76}$ and thus increased wall temperature causes the wall to be less catalytic; on the other hand, the proportionality of the gas-phase recombination rate to $\theta_w^{\omega-2}$ tends to freeze it out with increasing θ_w. The net result, as shown, is that both $Q_{w,f}$ and Q_w decrease away from $Q_{w,EQ}$ with increasing θ_w. Physically, we may understand these trends by noting that increased wall temperature has the effect of lowering the local density in the dominant cold gas layer near the surface, which correspond-

ingly reduces the reactive collisions between both the gas-phase atoms and the atoms on the wall surface.

The results of the fifth and final study, concerning the effect of flight velocity on nonequilibrium heating, are summarized in Fig. 11. Several opposing influences are at work in this case, resulting in the reversal of effect at higher velocities seen in the figure. At lower flight speeds, increase in U_∞ causes a strong increase in both H_D and ρ_s/ρ_∞ with little change in T_s, which thus rapidly increases both $Q_{w,EQ}$ and $Q_{w,F}$ [see Eqs. (22) and (23)]. Correspondingly, $\Gamma_c \sim [p_s/U_\infty T_s^{1.76}]^{1/2} \sim [U_\infty/T_s^{1.76}]^{1/2}$ is slowly reduced, gradually lowering the surface catalysis rate, where $\Gamma_G \approx [\rho_s(1+\alpha_s)]^2/U_\infty$ actually increases slightly (as confirmed by the detailed calculations), which moves Q_w gradually toward equilibrium. However, at a high enough U_∞ (approximately 9500 m/s in the present altitude example), these trends reverse: once dissociation becomes virtually complete ($\alpha_s \to 1$), further increase in U_∞ now causes T_s to rise significantly ($\sim U_\infty^2$ in fact) and so H_D and Γ_G start to reduce along with Γ_c, and, consequently, Q_w now reduces with U_∞ and begins to freeze out. This exercise brings out especially well the value of the present theory in understanding the underlying physics at observed parametric trends that would otherwise be difficult to discern from a purely numerical approach.

Concluding Remarks

The present investigation has shown that some appropriate simplifying approximations pertaining to highly cooled recombination-dominated chemistry can be exploited to develop a very convenient and efficient analytical method for prediction of nonequilibrium heat transfer in blunt-nose regions on arbitrarily catalytic hypersonic vehicles. The method lends itself especially well to cost-effective engineering design studies as illustrated by the various parametric study results presented here. Moreover, it yields significant physical insight into the processes in the stagnation-region boundary layer that govern diffusion, gas-phase reaction, and surface recombination. Finally, the developed solutions might also prove useful as initial conditions for viscous codes that predict the nonequilibrium flow downstream from the nose region.

Several extensions of this work would appear of value and are currently being explored. They are 1) inclusion of further nonequilibrium effects in the inviscid flow outside the boundary layer as encountered at very high altitude/high-speed flight conditions, and 2) addition of three-dimensional crossflow effects as they may alter the influence of nonequilibrium and surface catalycity on the boundary-layer heating. The latter would well serve the aerodynamic heating prediction needs of future hypersonic vehicles involving lifting configurations.

References

[1]Fay, J. A., and Riddell, F. R., "Theory of Stagnation-Point Heat Transfer in Dissociated Air," *Journal of the Aeronautical Sciences,* Vol. 25, No. 2, 1958, p. 73.

[2]Goulard, R. J., "On Catalytic Recombination Rates in Hypersonic Stagnation Heat Transfer," *Jet Propulsion,* Vol. 28, No. 11, 1958, pp. 737–745.

[3]Inger, G. R., "Nonequilibrium Stagnation-Point Boundary Layers with Arbitrary Surface Catalycity," *AIAA Journal,* Vol. 1, No. 8, 1963, pp. 1776–1783.

[4]Wittliff, S. E., and Curtis, J. T., "Normal Shock Wave Parameters in Equilibrium Air," Cornell Aeronautical Lab., Buffalo, NY, Rept. CAL-111, 1961.

[5]Marrone, P. V., "Normal Shock Waves in Air: Equilibrium Composition and Flow Parameters for Velocities from 26,000 to 50,000 ft/Sec," Cornell Aeronautical Lab., Buffalo, NY, Rept. AG-1729-A-2, 1962.

[6]Anon., "Normal and Oblique Shock Characteristics at Hypersonic Speeds," Douglas Aircraft Co., Long Beach, CA, Rept. LB-25599, 1957.

[7]Srinivasan, S., and Tannehill, J., "Simplified Curve Fits for the Transport Properties of Equilibrium Air," NASA CR-178411, Dec. 1987.